On Higher Order Dynamics in the Fundamental Equation of Frequency in Islanded Microgrids

J. Dobrowolski * **M. Alamir** ** **S. Bacha** *** **D. Gualino** *
M-X. Wang *

* *Schneider Electric Industrie. 37 Quai Paul Louis Merlin. 38000 Grenoble. (jean.dobrowolski(david.gualino(miao-xin.wang))@schneider-electric.com)*
** *CNRS, University of Grenoble Alpes. 11 rue des Mathmatiques, 38000 Grenoble, France (mazen.alamir@gipsa-lab.grenoble-inp.fr)*
*** *Laboratoire de Genie Electric de Grenoble. 21 avenue des Martyrs, 38000 Grenoble, France(Seddik.Bacha@g2elab.grenoble)*

Abstract: In islanded micro grids, the stability of the frequency has to be enhanced by the distributed producers. Moreover, distributed control schemes are highly appealing for evident robustness and flexibility reasons. This is generally achieved by using the fundamental frequency model in which the derivative of the grid frequency is proportional to the power unbalance in the grid. This paper discusses the relevance of this simple model when high gain closed-loop system is designed. In particular, the presence of higher order terms in the frequency dynamics that should be carefully taken into account in the distributed frequency control design is proved and appropriate frequency control law is proposed and validated.

Keywords: Microgrid, Decentralized control, Identification, Grid Frequency, DER, Control under Communication Constraints.

1. INTRODUCTION

Since the 2000s, the increasing awareness of environmental issues, combined with economic factors and the proliferation of distributed renewable resources enhanced an increasing interest in distributed grids (Zeh et al., 2016; Asmus, 2010; Hartono et al., 2013; Hatziargyriou et al., 2009; Bacha et al., 2015).

Microgrids are localized and autonomous electrical distribution networks composed of Distributed Energy Ressources (DER) including storage devices and loads. They can be connected to a larger power system or isolated voluntarily, to supply grid-off areas or islands (Jing et al., 2016), or involuntarily because of larger power blackout or disturbance (Hatziargyriou et al., 2007).

Islanded microgrids are composed of renewable energy producers which have to ensure grid stability, prompting a lot of research on frequency control (Tang et al., 2016; Reid, 2016; Simpson-Porco et al., 2015). Among others, the control based on the sole frequency measurement is an appealing concept to allow Plug & Play controlled architectures (Dörfler et al., 2014).

Due to the complexity of frequency dynamics of a whole microgrid and the targeted Plug & Play nature of their connection, the most common way to control frequency is to describe its dynamics as proportional to the unbalance between the total power P_p provided by the producers and the power P_l consumed by the loads (Delille et al., 2012; Zhao et al., 2016), namely:

$$\dot{f} = \alpha[P_p - P_l] \tag{1}$$

where α is a parameter that depends on the grid inertia. This equation comes from the approximation done when translating the swing equation from one generator to a multi-machine system leading to an equivalent generating unit describing the behavior of n generators (Anderson and Fouad, 2008; Rudez and Mihalic, 2011).

However, our recent investigation on real-life microgrid frequency control testbed suggested that an aggressive control (high closed-loop bandwidth) can destabilize the grid frequency which is not in accordance with what is expected, should the simplified frequency equation (1) be correct. This observation incited us to further investigate the structure of the frequency dynamics and the appropriate control gain design which is the main topics of the present contribution.

More precisely, we consider the model of a simple microgrid composed of two Gensets build up used the widely used PLECS toolbox of MATLAB/SIMULINK (Section 2). Based on this model and a concrete PLL-based grid frequency measurement, an identified dynamic model is derived for the variable $e = \dot{f} - \alpha(P_p - P_L)$ (Section 3). This variable obviously represents the dynamic of the error involved when using the simplified frequency equation (1). The results clearly show that a higher order model is necessary when high frequency dynamics are included in the sceanrios. In section 4, the resulting model is analyzed and the bandwidth limitation induced by the higher dynamics components of the new frequency model is discussed based on the recent results of (Alamir et al., 2017). It is in particular shown that necessary conditions can be derived for the parameter of frequency-measurement-based control law to enhance stability. Finally, Section 5 concludes the paper and gives the roadmap for further investigation.

2. SIMULATION MODEL

To identify the grid frequency dynamics, we need a simulator of a multisources microgrid. We choose to represent a microgrid composed of two gensets connected to a load. To analyze the behavior depending on the DERs size, we use one genset of 45kVA (MeccAlte, 2013) and one of 100kVA (Olympian, 2014) for a total microgrid power capacity of 145 kVA.

A genset is an autonomous system which is able to produce electricity, by transforming mechanical energy of a thermal engine into electrical energy via a synchronous machine. To simplify the complex modeling of synchronous machine (Zhong and Weiss, 2009), we choose to use PLECS-MATLAB toolbox which proposes a modeling block of synchronous machines whose behavior is explained in (PLECS, 2016).

The engine rotates at a speed ω which evolves proportionally to the unbalance between the mechanical torque Γ_m applied by a motor and the electromagnetic torque Γ_e required by load via the synchronous machine. Namely

$$J\frac{d\omega}{dt} = \Gamma_m - \Gamma_e - D\omega \tag{2}$$

where J is the inertia and D is the damping coefficient. Sum of producers mechanical torque without damping $(\Gamma_m - D\omega)$ is the mechanical image of P_p and sum of electromagnetic torque Γ_e is the mechanical image of P_l. The engine rotational speed ω is associated to the genset frequency $f = (N\omega)/(2\pi)$ with N the number of poles of the synchronous machine.

To ensure a balanced sharing of the load power among DERs, and to control frequency in case of an islanding microgrid, the well know primary droop control is used (Simpson-Porco et al., 2015; Zhong, 2013). Primary control is based on the active/reactive power decoupling (Zhong, 2013) and calculates a rotational speed reference ω_{ref} in order to keep (P_m, ω) on the droop line defined by

$$\omega = \omega_0 - m \times P \tag{3}$$

where ω_0 is the nominal grid frequency and m is the droop slope. The rationale behind the droop characteristic is that an increase of the measured power P_m is the sign of an increase of the load power P_l which should induce a drop in the frequency (following the basic presumed dynamics (1)) in order to increase and share the total produced power P_p between each producers.

Note that in the presence of two gensets, the direct link between the grid frequency f and the rotational speed ω is no more a priori valid since now we have two $\omega_i s$ that cannot be instantaneously equal. Instead, the grid frequency is evaluated using a Phase Lock Loop (PLL) designed as explained in (Hadjidemetriou et al., 2013). This commonly admitted technique is used in the simulator to deliver the grid frequency for the forthcoming identification step. This results in the simulation framework depicted in figure 3.

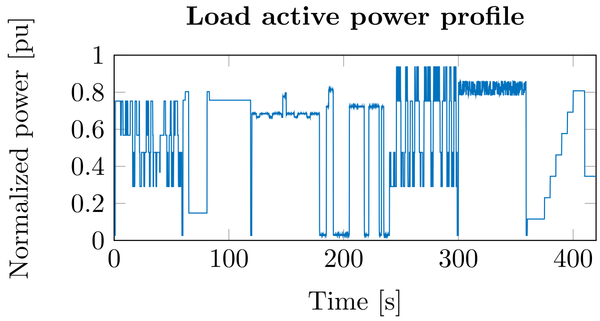

Figure 1. Normalized load active power profile for the scenario used in the identification of the grid frequency dynamics.

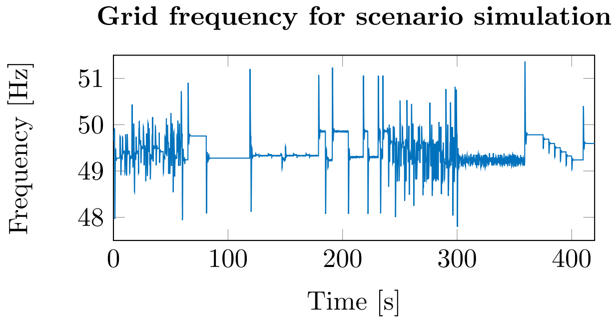

Figure 2. The frequency evolution during the identification scenario in response to the active power load profile of Figure 1.

Figure 1 shows the load power scenario normalized by the total power capacity of the gensets. Figure 2 shows the corresponding PLL-based measurements of the grid frequency f during the identification scenario.

3. DYNAMIC FREQUENCY MODEL

Now that we defined a microgrid simulator and an identification scenario, our aim is to investigate to which extent does the simplified dynamics (1) represent the measured frequency in the simple two gensets micro grid described in the preceding section.

Figure 4 checks the validity of the basic equation (1) by comparing $\dot{f}$ to $\alpha(P_p - P_\ell)$ where α is computed to give a better possible fit. The latter is defined as follows:

$$\text{fit} = \left[1 - \sum_{t=1}^{t_{max}} \frac{|\dot{f}(t) - \alpha(P_p(t) - P_l(t))|}{|\dot{f}(t)| + \varepsilon}\right] \times 100 \tag{4}$$

From Figure 4, it can be clearly observed that the basic equation (1) is not sufficient to capture the transient in the measured frequency and that a higher order model seems to be necessary.

Considering the residual

$$e = \dot{f} - \alpha(P_p - P_\ell) \tag{5}$$

of the satisfaction of the basic frequency equation (1) as the output of a dynamical system to be identified and the derivative of the total produced power and load power, namely $\dot{P}_p$ and $\dot{P}_\ell$ as input signals, it is possible to use a state-space identification subroutines such as the MAT-

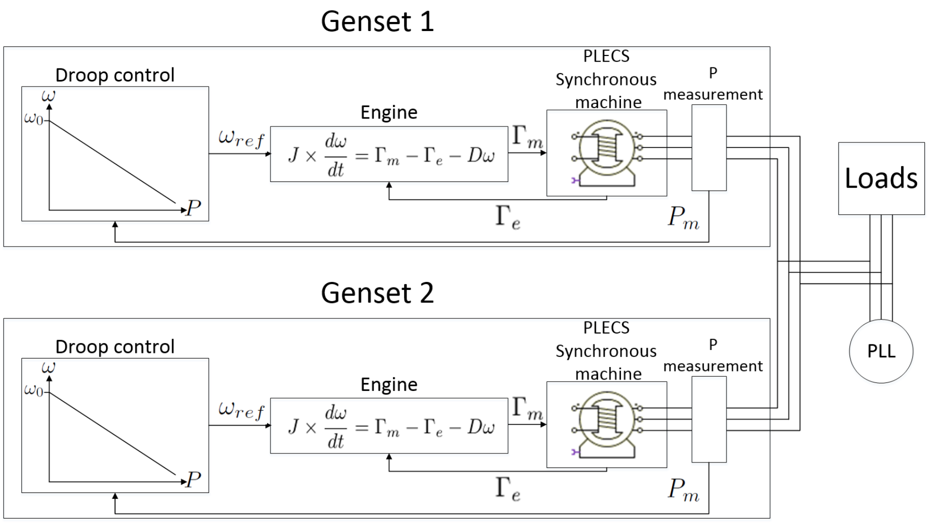

Figure 3. Schematic view of the simulation used to identify the two-gensets grid frequency dynamics.

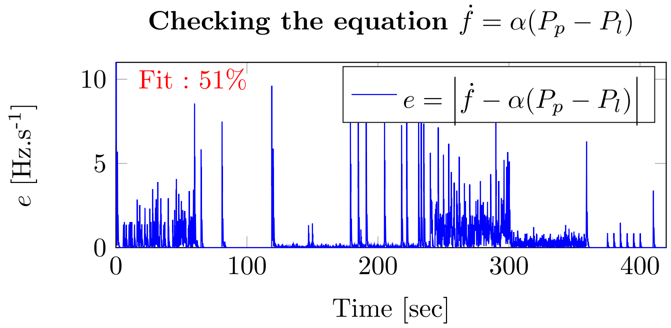

Figure 4. Checking the equation $\dot{f} = \alpha(P_p - P_\ell)$: Comparison between $\dot{f}$ and the best fit of $\alpha(P_p - P_\ell)$.

LAB/N4SID in order to derive an identified input/output system of the following form:

$$\dot{\eta} = A\eta + Bu \quad \text{where} \quad u := \begin{bmatrix} \dot{P}_p \\ \dot{P}_\ell \end{bmatrix} \tag{6}$$

$$e = C\eta + Du \tag{7}$$

Figure 5 shows the identification results using the criterion (4) for different presumed orders for the dynamics used in (6). The plots suggest that a 5-th order model is needed in order to faithfully represents the dynamics of the residual

Combining (5) with (6)-(7) in which the input/output gain matrix $D = 0$ (by the identification results), the complete identified dynamics of the grid frequency can be given by:

$$\dot{\eta} = A\eta + B_1\dot{P}_p + B_2\dot{P}_l \tag{8}$$

$$\dot{f} = \alpha(P_p - P_l) + C\eta \tag{9}$$

Examination of the eigenvalues of the state matrix A involved in the resulting model (8) shows that this matrix is Hurwitz with oscillating modes. Figure 6 shows the impulse response of (7). The real system input is the load power P_l so there is no sense to apply impulse directly on $(\dot{P}_p - \dot{P}_l)$ because P_p and P_l are linked by mechanical equation. It comes clearly that the settling time of the second term in (9) which represents the error of the commonly used simple dynamics (1) has an order of magnitude of 1.5 sec.

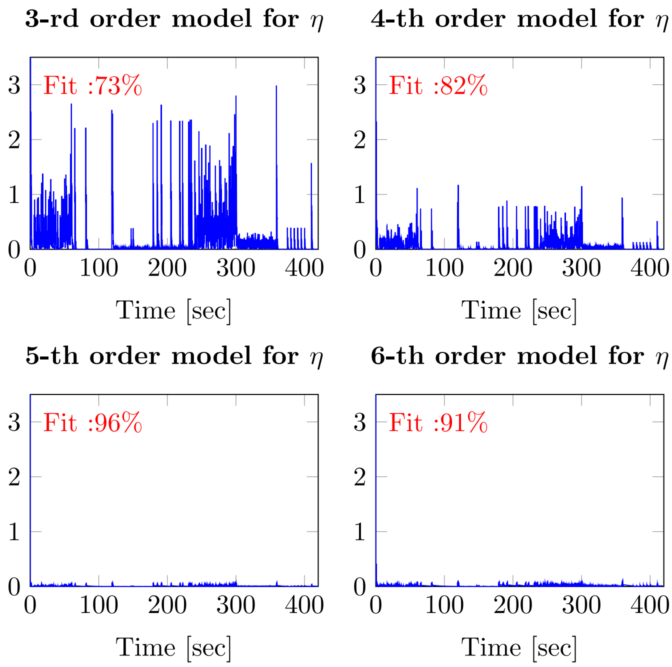

Figure 5. Evolution of the identification error on the residual $e = \dot{f} - \alpha(P_p - P_l)$ for different orders of the identified dynamics (6). The plots suggest that a 5-th order model is needed in order to faithfully represent the dynamics of the residual and hence to provide a representative model (8)-(9) for the grid frequency dynamics.

This explains why an agressive closed-loop control that ignores the presence of this extra dynamics can destabilize the behavior of the frequency. This destabilizing effect is accentuated by the fact that the derivative of the produced power $\dot{P}_p$ (that is viewed as the control variable in the frequency stabilizing feedback) is precisely the leading term in (8) that excites the *internal state* η of the frequency dynamics once the variation of the load power stops.

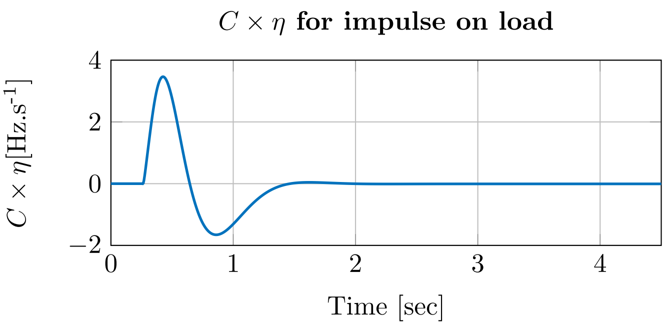

Figure 6. Impulse response of (8) for an impulse on the load power P_ℓ.

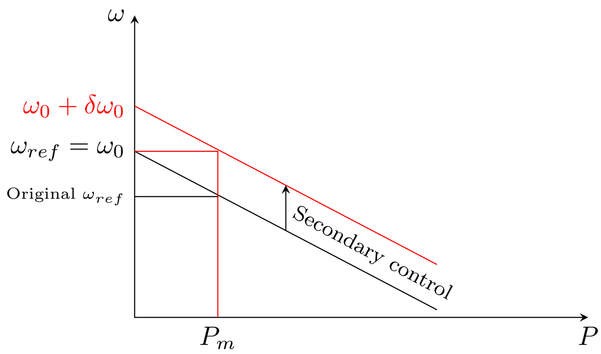

Figure 7. Droop with secondary control

4. DISCUSSION

Recall that we are interested in output feedback control that regulates the grid frequency around its reference value $f_0 \Leftrightarrow \omega_0$ (typically 50Hz). To do so, we follow the suggestion by (Simpson-Porco et al., 2015) by adding a secondary control $\delta\omega_0$ that modifies the offset ω_0 of the droop characteristic of equation (3). By doing so, the reference value ω_{ref} is shifted by $\delta\omega_0$ (see 7) which becomes the so-called secondary control variable that manipulates the power produced by each individual Genset.

In order to regulate the frequency of the extended model (8)-(9), the total power that producers have to provide P_p has to be estimated. This global estimation allows to share P_p between producers and to compute the secondary control variable $\delta\omega_0$. Considering that all producers have the same droop slope m, we share P_p equitably relative to producers size by applying the following secondary control :

$$\delta\omega_{0_i} = m \times P_p \times \frac{P_i}{\overline{P}} \tag{10}$$

with $\overline{P}$ the total power of all producers, P_i the size of i$^{\text{th}}$ producer and $\delta\omega_{0_i}$ its secondary control variable.

Assuming that P_p is bounded by the grid capacity $[P_{min}, P_{max}]$, we use the control law proposed in (Alamir, 2015) and (Alamir et al., 2017), namely:

$$P_p = S\left(\lambda(f_0 - f) + z\right) \tag{11a}$$

$$\dot{z} = \lambda_f \left(P_p - z\right) \tag{11b}$$

With λ and λ_f two design parameters, z the internal state of the controller while S the saturation function according to $S(v) =$:

$$S(v) := \min\{P_{max}, \max\{P_{min}, v\}\} \tag{12}$$

Note that the dynamics is steered only by the measured signal f and the internal state z. Therefore, they can be *run* by all the gensets so that they can have a common estimation z of the load power.

Note that in (Alamir, 2015), it has been shown that if (1) were true, there would be no theoretical limitation on λ and therefore one can control the frequency as tightly as desired. On the other hand, (Alamir et al., 2017) investigated the case where internal dynamics is present and derived appropriate bounds on λ and λ_f that leads to a controlled closed-loop performance. These two situations are analyzed in the next sections for the micro grid context while (Alamir, 2015) and (Alamir et al., 2017) give general purpose results.

4.1 Without limitation on control gains

The design proposed in (Alamir, 2015) holds for (1) provided that $\alpha \in [\underline{\alpha}, \overline{\alpha}]$, $P_l \in [P_{lmin}, P_{lmax}]$ such that:

$$P_{max} - P_{lmax} \geq \varrho_+ > 0 \tag{13}$$

$$P_{lmin} - P_{min} \geq \varrho_- > 0 \tag{14}$$

These assumptions hold for the micro grid case with $P_p \in [0, 145]$ kW , $P_l \in [3.5, 121.8]$ kW and $\alpha \in [0.1, 1]$.

Under these conditions, (Alamir, 2015) states that if (1) holds then for any $\lambda > 0$, if the following conditions hold:

$$\lambda_f < \left[\min\left\{\frac{\min\{\varrho_+, \varrho_-\}}{P_{max} - P_{min}}, \frac{\underline{\alpha}}{4}\right\}\right] \times \lambda \tag{15}$$

$$\left|\frac{dP_l}{dt}\right| \leq \sigma_{P_l} \tag{16}$$

then the dynamic feedback law defined by (11) leads to a tracking error $e_f = f - f_0$ such that

$$\lim_{t\to\infty} |e_f| \leq \frac{\sigma_{P_l}}{\lambda \times \lambda_f} \tag{17}$$

For the scenario of Figure 2, one has $\sigma_{P_\ell} \leq 510500$ and $\min\left\{\frac{\min\{\varrho_+, \varrho_-\}}{P_{max} - P_{min}}, \frac{\underline{\alpha}}{4}\right\} = 0.0241$. Therefore, to ensure an asymptotic tracking error lower that 0.1 Hz, the conditions on λ is:

$$\frac{\sigma_{P_l}}{\lambda \times \lambda_f} \leq 0.1 \Leftrightarrow \lambda \geq \sqrt{\frac{510500}{0.0241 \times 0.1}} = 14554 \tag{18}$$

Figure 8 shows a simulation of the closed-loop system (1) under (11) with $\lambda = 14600$ and $\lambda_f = 14600 \times 0.0240$. It can be observed that the predicted asymptotic bound on the tracking error holds.

Unfortunately, the simulation of the identified high order system (8)-(9) using the same law (11) in which the same (λ, λ_f) are used shows very bad behavior as it can be observed in Figure 9. This comes from the fact that the high gain $\lambda = 14554$ induces high oscillations on η [through (8)] which is then injected in the frequency equation (9) making uncontrollable the dynamics of the frequency. Fortunately, the framework of (Alamir et al., 2017) precisely tackles this issue as it is shown in the next section.

4.2 With limitation on control gains

This section heavily involves the recent results of (Alamir et al., 2017) whose full statement lies beyond the scope

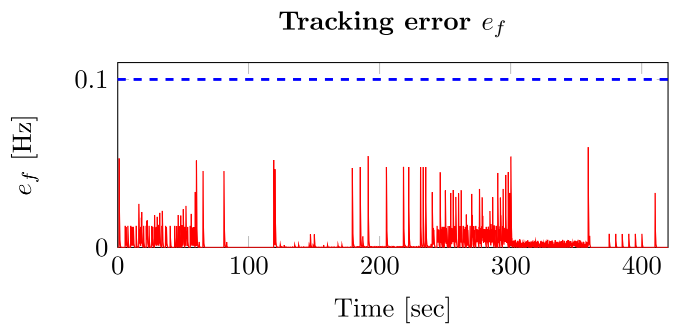

Figure 8. Tracking error and estimation error of closed loop of (1) and (11) with $\lambda = 14600$ and $\lambda_f = 350.4$

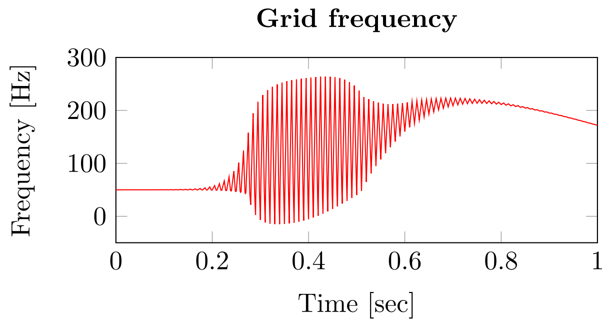

Figure 9. Grid frequency of closed loop of (9) and (11) with $\lambda = 14600$ and $\lambda_f = 350.4$

of the present contribution. The general equation of the proposed theory is :

$$\dot{y} = \alpha\left(P_p - P_l + \frac{C\eta}{\alpha}\right) \tag{19}$$

Therefore performance of control will be strongly linked to the lowest bound of α the denominator of $C\eta$. To fix this value, we consider a design variable γ in the system:

$$\dot{\bar{y}} = \frac{\dot{y}}{\gamma} = \alpha\left(\frac{P_p}{\gamma} - \frac{P_l}{\gamma} + \frac{C\eta}{\alpha\gamma}\right) \tag{20}$$

Stability of (19) is satisfied if that of (20) is satisfied considering γ as a time scale variable.

Only the main guidelines of the result are developed.

Note first of all that one obviously has:

$$\left|\frac{C\eta(t)}{\alpha\gamma}\right| \leq c_0 + c_1||\frac{\dot{u}}{\gamma}||_\infty \tag{21}$$

$$\left|\frac{C\dot{\eta}(t)}{\alpha\gamma}\right| \leq d_0 + d_1||\frac{\dot{u}}{\gamma}||_\infty \tag{22}$$

where c_0, c_1, d_0 and d_1 are given by:

$$c_0 := \epsilon + \sup_{t\geq 0}\left|\frac{C}{\alpha\gamma}\int_0^t \exp^{A(t-\sigma)} B_2 \frac{\dot{P}_l}{\gamma} d_\sigma\right| \tag{23a}$$

$$c_1 := \sup_{t\geq 0}\left|\frac{C}{\alpha\gamma}\int_0^t \exp^{A(t-\sigma)} B_1 d_\sigma\right| \tag{23b}$$

$$d_0 := \epsilon + \sup_{t\geq 0}\left|\frac{C}{\alpha\gamma}A\int_0^t \exp^{A(t-\sigma)} B_2 \frac{\dot{P}_l}{\gamma} d_\sigma\right| + \left|\frac{C}{\alpha\gamma}B_2\frac{\dot{P}_l}{\gamma}\right| \tag{23c}$$

$$d_1 := \sup_{t\geq 0}\left|\frac{C}{\alpha\gamma}A\int_0^t \exp^{A(t-\sigma)} B_1 d_\sigma\right| + \left|\frac{C}{\alpha\gamma}B_1\right| \tag{23d}$$

Under (21)-(22), together with the bounds on α, P_ℓ and P_p, one can rephrase the main result of (Alamir et al., 2017) by stating that **if the following conditions hold**:

(1) $c_0 < \min\{\frac{\varrho^-}{\gamma}, \frac{\varrho^+}{\gamma}\}$

(2) $\lambda < \lambda^*$ where λ^* is given by:

$$\lambda^* = \sup\left\{\sigma < \frac{1}{\bar{\alpha}c_1}\,\middle|\, \inf_{\lambda\in(0,\sigma)}\phi(\lambda) \leq 0\right\} \tag{24}$$

in which ϕ is defined according to:

$$\phi(\lambda) = \frac{\left[\frac{\underline{\varrho}}{\gamma} - c_0 - \lambda\frac{\left(\frac{\beta}{\gamma} + c_0\right)c_1\bar{\alpha}}{1 - \lambda\bar{\alpha}c_1}\right]\underline{\alpha}}{\left[\frac{\Delta_P}{\gamma}\left(1 + \frac{\lambda c1\underline{\alpha}}{1-\lambda\bar{\alpha}c_1}\right)\right]} \tag{25}$$

where $\Delta_P = P_{max} - P_{min}$, $\underline{\varrho} = \min\{\varrho^-, \varrho^+\}$ and $\beta = P_{lmax} - P_{lmin} + \max\{\varrho^-, \varrho^+\}$.

(3) $\lambda_f < \lambda \times \phi(\lambda)$

(4) The dynamic of P_l respect $\left|\frac{dP_l}{dt}\right| \leq \frac{\sigma_{P_l}}{\gamma}$

Then according to (Alamir et al., 2017) the stability of (20) is satisfied and so **the tracking error e_f of system (19) with control (11) satisfies**:

$$\lim_{t\to\infty}|e_f| \leq \frac{\sigma_{P_l} + d_0 + d_1\sigma_u}{\lambda\times\lambda_f} \tag{26}$$

where σ_u is given by:

$$\sigma_u = \frac{\lambda\bar{\alpha}\left[\beta + c_0\right] + \lambda_f\Delta_u}{1 - \lambda\bar{\alpha}c_1} \tag{27}$$

Using the identified system (8) and (9) $c_0 = 2.456 \times 10^{-2}$, $c_1 = 1.156 \times 10^{-4}$, $d_0 = 3.8754 \times 10^{-2}$ and $d_1 = 2.435 \times 10^{-4}$ with $\gamma = 70$. The definition of λ^* is obtained through the evolution of the function $\phi(\lambda)$ depicted in Figure 10. Indeed, This figure clearly shows that $\lambda^* = 1400$ (maximum value of λ such that $\phi(\lambda) \geq 0$). Using $\lambda = 0.8\lambda^* = 1120$ leads to $\lambda_f = \phi(\lambda)\lambda = 34$. Injecting these values in (26)-(27) gives the guaranteed asymptotic bound $\lim_{t\to\infty}|e_f| \leq 1.3$ which is confirmed by the simulation of Figure 11. Note that this bound holds even if P_ℓ keep varying continuously. If P_ℓ becomes constant, the bound is given by $\lim_{t\to\infty}|e_f| \leq 0.13$

Note that as many theoretical bounds, the asymptotic bound predicted by the theory is an upper pessimistic bound that is based on many worst-case inequalities used in the derivation of the theoretical statement. It gives however a safety bound that the practitioner can use with confidence in the choice of the control parameters design.

5. CONCLUSION AND FUTURE WORK

In this paper, the problem of distributed control of frequency in micro grids is investigated. In particular, it has been shown that the fundamental equation of frequency in micro grids is only valid for a limited bandwidth beyond which high order dynamics have to be taken into account in the control design. Moreover, an appropriate recently developed framework (Alamir et al., 2017) has been adapted to the micro grid context leading to a simple dynamic

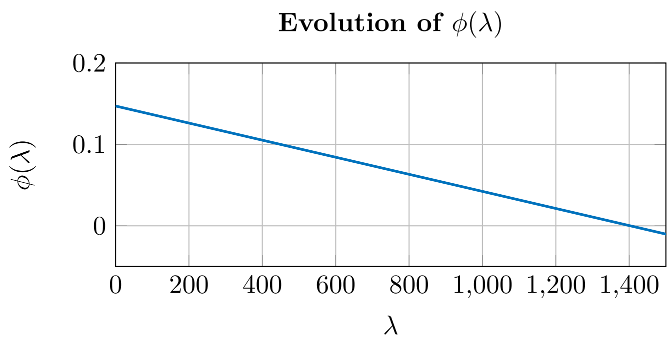

Figure 10. behavior of $\phi(\lambda)$ in use case

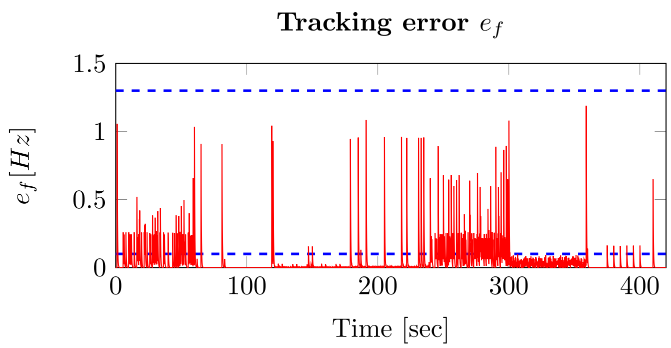

Figure 11. Tracking error of closed-loop of (9) and (11) with $\lambda = 1120$ and $\lambda_f = 34$. Dotted lines represents the bounds 1.3 and 0.1 corresponding to continuously varying P_ℓ and $\dot{P}_\ell = 0$

output feedback design with the associated bounds on the control gains. The whole framework has been validated on a simple two-genset micro grid.

Future investigation concerns the application of the main result to a real-life tested that is currently under construction at Schneider Electric company.

REFERENCES

Alamir, M. (2015). On Controlling Unknown Scalar Systems with Low Gain Feedback. Research report, GIPSA-lab. URL `https://hal.archives-ouvertes.fr/hal-01215808`.

Alamir, M., Jean, D., and Mohamed, A.T. (2017). Output Feedback Control of a Class of Uncertain Systems Under Control-derivative dependent disturbances. In *IFAC World Congress*. Toulouse, France.

Anderson, P.M. and Fouad, A.A. (2008). *Power system control and stability*. John Wiley & Sons.

Asmus, P. (2010). Microgrids, virtual power plants and our distributed energy future. *The Electricity Journal*, 23(10), 72–82.

Bacha, S., Picault, D., Burger, B., Etxeberria-Otadui, I., and Martins, J. (2015). Photovoltaics in microgrids: An overview of grid integration and energy management aspects. *IEEE Industrial Electronics Magazine*, 9(1), 33–46.

Delille, G., Francois, B., and Malarange, G. (2012). Dynamic frequency control support by energy storage to reduce the impact of wind and solar generation on isolated power system's inertia. *IEEE Transactions on Sustainable Energy*, 3(4), 931–939.

Dörfler, F., Simpson-Porco, J.W., and Bullo, F. (2014). Plug-and-play control and optimization in microgrids. In *53rd IEEE Conference on Decision and Control*, 211–216.

Hadjidemetriou, L., Kyriakides, E., and Blaabjerg, F. (2013). A new hybrid pll for interconnecting renewable energy systems to the grid. *IEEE Transactions on Industry Applications*, 49(6), 2709–2719.

Hartono, B., Budiyanto, Y., and Setiabudy, R. (2013). Review of microgrid technology. In *QiR (Quality in Research), 2013 International Conference on*, 127–132.

Hatziargyriou, N.D., Anastasiadis, A.G., Vasiljevska, J., and Tsikalakis, A.G. (2009). Quantification of economic, environmental and operational benefits of microgrids. In *PowerTech, 2009 IEEE Bucharest*, 1–8.

Hatziargyriou, N., Asano, H., Iravani, R., and Marnay, C. (2007). Microgrids. *IEEE power and energy magazine*, 5(4), 78–94.

Jing, H., Xiaohua, L., and Hongping, L. (2016). Control method of islanded microgrid to improve reactive power sharing and power quality. In *2016 China International Conference on Electricity Distribution (CICED)*, 1–5.

MeccAlte (2013). Datasheet generator type ecp 32-3s/4 a.

Olympian (2014). Datasheet of diesel generator gep110-4.

PLECS (2016). PLECS user manual. `www.plexim.com/files/plecsmanual.pdf`.

Reid, D. (2016). Ems control of reduced energy storage capacity for ramp rate support to improve frequency regulation in islanded microgrid. In *SoutheastCon 2016*.

Rudez, U. and Mihalic, R. (2011). Monitoring the first frequency derivative to improve adaptive underfrequency load-shedding schemes. *IEEE Transactions on Power Systems*, 26(2), 839–846.

Simpson-Porco, J.W., Shafiee, Q., Dörfler, F., Vasquez, J.C., Guerrero, J.M., and Bullo, F. (2015). Secondary frequency and voltage control of islanded microgrids via distributed averaging. *IEEE Transactions on Industrial Electronics*, 62(11), 7025–7038.

Tang, X., Hu, X., Li, N., Deng, W., and Zhang, G. (2016). A novel frequency and voltage control method for islanded microgrid based on multienergy storages. *IEEE Transactions on Smart Grid*, 7(1), 410–419.

Zeh, A., Rau, M., and Witzmann, R. (2016). Comparison of decentralised and centralised grid-compatible battery storage systems in distribution grids with high pv penetration. *Progress in Photovoltaics: Research and Applications*, 24(4), 496–506. PIP-14-162.R1.

Zhao, J., Lyu, X., Fu, Y., Hu, X., and Li, F. (2016). Coordinated microgrid frequency regulation based on dfig variable coefficient using virtual inertia and primary frequency control. *IEEE Transactions on Energy Conversion*, 31(3), 833–845.

Zhong, Q. and Weiss, G. (2009). Synchronverters: Inverters that mimic synchronous generator. *IEEE Power Engineering Society Power Systems Conference & Exhibition*.

Zhong, Q.C. (2013). Robust droop controller for accurate proportional load sharing among inverters operated in parallel. *IEEE Transactions on Industrial Electronics*, 60(4), 1281–1290.